Published in final edited form as:
*Cytoskeleton (Hoboken)*. 2010 January ; 67(1): 43–55. doi:10.1002/cm.20423.

# Changes in plasma membrane structure and electromotile properties in prestin deficient outer hair cells

**David Z.Z. He**[1], **Shuping Jia**[1], **Takashi Sato**[2], **Jian Zuo**[3], **Leonardo R. Andrade**[2], **Gavin P. Riordan**[2], and **Bechara Kachar**[2,*]

[1]Department of Biomedical Sciences, Creighton University School of Medicine, Omaha, NE 68178

[2]Laboratory of Cell Structure and Dynamics, National Institute on Deafness and Other Communication Disorders, NIH, Bethesda, MD 20892

[3]Department of Developmental Neurobiology, St Jude Children's Research Hospital, Memphis, TN 38105

## Abstract

Cochlear outer hair cells (OHCs) rapidly change their length and stiffness when their membrane potential is altered. Prestin, the motor protein for this electromotility, is present along the OHC lateral plasma membrane where there is a high density of intra-membrane protein particles (IMPs). However, it is not known to what extent prestin contributes to this unusual dense population of proteins and overall organization of the membrane to generate the unique electromechanical response of OHCs. We investigated the relationship of prestin with the IMPs, the underlying cortical cytoskeletal lattice, and electromotility in prestin-deficient mice. Using freeze-fracture, we observed a reduction in density and size of the IMPs that correlates with the reduction and absence of prestin in the heterozygous and homozygous mice, respectively. We also observed a reduction or absence of electromotility-related charge density, axial stiffness, and piezoelectric properties of the OHC. A comparison of the charge density with the number of IMPs suggests that prestin forms tetramers in the wild type but is likely to form lower number oligomers in the prestin-deficient OHCs from the heterozygous mice. Interestingly, the characteristic actin-based cortical cytoskeletal lattice that underlies the membrane is absent in the prestin-null OHCs, suggesting that prestin is also required for recruiting or maintaining the cortical cytoskeletal lattice. These results suggest that the majority of the IMPs are indeed prestin and that electrically evoked length and stiffness changes are interrelated and dependent on both prestin and on the cortical actin cytoskeletal lattice of the OHC lateral membrane.

### Keywords

Outer hair cell motility; electromotility; prestin; hair cell; membrane cytoskeleton; cortical lattice

## INTRODUCTION

The outer hair cell, one of the two mechano-electrical sensory cell types in the organ of Corti, generates a mechanical feedback that is part of the cochlear amplification mechanism. Early work showed that OHCs are able to change their length when their membrane

[*]**Correspondence To:** Bechara Kachar, NIDCD, National Institutes of Health, 50 South Drive, Rm 4249, Bethesda, MD 20892-8027, karcharb@nidcd.nih.gov or David Z.Z. He, Creighton University School of Medicine, 2500 California Plaza, Omaha, NE 68178, Tel.: (402) 280-1409 Fax.: (402) 280-3690, hed@creighton.edu.

potential is altered (Brownell et al. 1985; Brownell and Kachar 1985; Goldstein and Mizukoshi 1967; Kachar et al. 1986a; Zenner et al. 1985). This contractile response was shown to be a novel ATP-independent form of cell motility (Kachar et al. 1986a) generated along the OHC lateral membrane (Kalinec et al. 1992), where a unique high density of large intramembrane protein particles (IMPs) are observed by freeze-fracture electron microscopy (Gulley and Reese 1977). A hallmark of this electrically evoked motile response or electromotility is a measurable voltage dependent, non-linear membrane capacitance (Ashmore 1989; Santos-Sacchi 1991), which results from charge movements analogous to those observed for gating charge movements of voltage dependent ion-channel proteins. A membrane protein named prestin has been identified as the motor protein for OHC electromotility (Zheng et al. 2000). Intracellular anions are proposed to be the voltage sensor (Oliver et al. 2001). Prestin is located in the OHC lateral membrane (Adler et al. 2003; Belyantseva et al. 2000a) along the region of high IMP density. A well-organized actin-based cortical cytoskeleton, called cortical lattice (Holley and Ashmore 1988; Holley et al. 1992), and a continuous network of smooth endoplasmic reticulum called subsurface cisternae, underlie this unique region of the lateral plasma membrane to form an integrated structural complex know as the OHC lateral wall. The lateral wall, together with turgor pressure, provides support for the cylindrical cell shape and contributes to the overall passive mechanical properties of the OHC. In addition to length changes, OHCs exhibit voltage dependent axial stiffness changes (Frolenkov et al. 1998b; He and Dallos 1999). It has been proposed that these two processes depend on the voltage-dependent properties of prestin (He et al. 2003).

Previous studies show that time course of prestin expression correlates with the development of electromotility (Belyantseva et al. 2000a; He et al. 1994) and with an increase in IMP density (Souter et al. 1995). However, it is not clear how prestin contributes to the high density of large IMPs since other proteins are present in this region of the OHC lateral plasma membrane (Belyantseva et al. 2000b; Geleoc et al. 1999). It is also not clear to what extent prestin oligomerizes and whether prestin contributes to the recruitment and organization of the cortical lattice. While several theoretical models regarding how OHC length and stiffness changes are generated have been proposed (Dallos and He 2000; Iwasa 2000), there is no direct evidence for how prestin promotes length and stiffness changes and how these two processes are linked. In this study, we used prestin-deficient mice to examine the density and size distribution of IMPs in the plasma membrane, the overall organization of the lateral wall, and the electromechanical properties of the OHCs.

## MATERIAL AND METHODS

All animal experiments were carried out according to Creighton University, St. Jude Children's Research Hospital, and NIH (protocol # 1215-06) approved guidelines for ethical treatment of laboratory animals. Minima of 3 mice (aged between 18 and 30 days after birth) for each genotype and for each procedure were analyzed. Since progressive hair cell loss started from the basal turn after 24 days in the prestin knockout mice (Liberman et al., 2002; Wu et al., 2004), all the hair cells used for the experiments were obtained from the apical turn of the cochleae.

### Measurement of nonlinear capacitance

OHCs were isolated using enzymatic digestion and gently stirred using a pipette with large bore, and bathed in an extracellular solution containing (in mM) 120 NaCl, 20 TEA-Cl, 2 $CoCl_2$, 2 $MgCl_2$, 10 HEPES, and 5 glucose, at pH 7.3. The internal solution contained 140 CsCl, 2 $MgCl_2$, 10 EGTA, and 10 HEPES at pH 7.3 to block voltage-dependent ion channels in the basolateral membrane, thereby isolating the capacitive current. After whole-cell voltage-clamp recording was established at room temperature (20±2°C), a two-sine

voltage stimulus protocol (10 mV peak at both 390.6 and 781.2 Hz) with subsequent fast Fourier transform-based admittance analysis was used to measure membrane capacitance(Santos-Sacchi et al. 2001) from a holding potential of 0 mV. The capacitive currents were sampled at 100 kHz and low-pass filtered at 5 kHz. Series resistance was compensated off-line. Data were acquired using jClamp (Scisoft, New Haven, CT) and analyzed with Igor (WaveMetrics, Portland, OR).

The nonlinear capacitance can be described as the first derivative of a two-state Boltzmann function relating nonlinear charge movement to voltage (Ashmore, 1989; Santos-Sacchi, 1991). The capacitance function is described as:

$$C_m = \frac{Q_{\max}\alpha}{\exp[\alpha(V_m - V_{1/2})](1+\exp[-\alpha(V_m - V_{1/2})])^2} + C_{lin}$$

where $Q_{max}$ is maximum charge transfer, $V_{1/2}$ is the voltage at which the maximum charge is equally distributed across the membrane, or equivalently, the peak of the voltage-dependent capacitance, $C_{lin}$ is linear capacitance, and $\alpha = ze/kT$ is the slope of the voltage dependence of charge transfer where $k$ is Boltzmann's constant, $T$ is absolute temperature, $z$ is valence of charge movement, and $e$ is electron charge.

## Measurement of OHC axial stiffness

Cell motility and fiber motion were measured by a photodiode-based system. The magnified image of the OHC's apical membrane or the fiber was projected onto the photodiode through a rectangular slit. The position of the slit in front of the photodiode was adjustable so that the image of the object could always be projected onto the photodiode without moving the cell or the fiber. Cell-length changes or fiber displacements were measured by changes in the current of the photodiode. The photocurrent response was calibrated to displacement units by moving the slit by a fixed distance (0.5 μm) with the image of the cell (or fiber) at the beginning of each trial. The measuring system's 3-dB cutoff frequency was at 1100 Hz. The photocurrent responses were sampled at 50 kHz. Ten averages were usually preset for each trial. Data were acquired using pClamp (Molecular Devices, Sunnyvale, CA) and analyzed by Igor programs (WaveMetric).

The axial stiffness of OHCs was measured under the voltage-clamp condition as described elsewhere (He and Dallos 1999). Glass fibers were pulled from 1.5 mm glass tubing using a microforge (Narashige, East Meadow, NY). The tapered tip of a fiber was usually 4–5 mm in length and 2–3 μm in diameter. Fiber stiffness ranged between 1.2 and 3.8 mN/m and was calibrated using the technique introduced by Howard and Ashmore (Howard and Ashmore 1986). The tip of the glass fiber was brought against the cuticular plate of the cell held at the holding potential of −70 mV. The fiber was placed transverse to the OHC's long axis so that the fiber's lateral motions would compress or relax the cell. The fiber motions were measured and calibrated by a photodiode-based measurement system. Several parameters were measured. These were "unloaded motility," the measurement of the cells' electrically induced motile displacement response without loading by the fiber; "unloaded-fiber" motion, the displacement of the tip of the fiber when driven by the bimorph but not loaded by the cell; and "loaded response," the joint displacement of the junction between cell and fiber after loading. The axial stiffness ($k_c$) of the cell was computed by comparing the free movement ($L_f$) of the tip of the fiber of known stiffness ($k_f$) with the loaded movement ($L_c$) of the tip after it was rested against the surface of the cuticular plate, where: $k_c = k_f(L_f - L_c)/L_c$.

### Electron microscopy

For conventional thin section or for freeze-fracture electron microscopy, mice (three per genotype) were deeply anesthetized, decapitated, and had the cochlea removed and fixed for two hours by immersion in 2.5 % glutaraldehyde, 4% paraformaldehyde in PBS at room temperature. For freeze-fracture, fixed samples were glycerinated (30%), plunge-frozen in Freon 22 cooled in liquid nitrogen, fractured, and replicated at 45° degrees with platinum/carbon in a Balzers apparatus as previously described (Kachar et al. 1986b). For immunogold labeling, samples were fixed in 4% paraformaldehyde in PBS for 2 h, then glycerinated (30%) and plunge-frozen in Freon 22 cooled in liquid nitrogen. Frozen tissues were freeze-substituted in an automated freeze-substitution apparatus (Leica, Germany) with 1% uranyl acetate in methanol at −90°C for 2 days, embedded in Lowicryl (EMS,Hatfield, PA) at −20°C for 1 day, and polymerized in UV light at −20°C for 2 days. Immunogold labeling was performed on thin sections as previously described (Dumont et al. 2001; Nunes et al. 2006; Salles et al. 2009). The antibody specific to prestin used was PB121, which was raised against a portion of the C-terminus of the prestin as described in Belyantseva et al. (Belyantseva et al. 2000a). Control experiments for the post embedding immunogold-labeling shows no labeling along the lateral plasma membrane when using an antibody unrelated to prestin (PB288). More importantly, PB121 does not label inner hair cells or diter cells (data not shown) as well as it does not label the OHCs in prestin KO mice tissue. All samples were viewed and photographed with either a JEOL100 or a Zeiss 922 transmission electron microscope. ImageJ (NIH) and Igor software were used for image and data analyses. For the quantification of prestin labeling, gold particles were counted along ~30 linear segments of cross-sectioned lateral plasma membrane from OHCs obtained from three mice per genotype. Measurement of intramembrane particle sizes in freeze-fracture replicas from at least three mice per genotype was performed by measuring the diameter of particles perpendicular to the direction of the platinum shadow to avoid variations due to differences of angle of shadow.

### Data Analysis

All values were presented as Means ± S.D.. The Student’s unpaired t test was applied, and $P<0.05$ was considered statistically significant. One-Sample T Test was also used to determine whether the mean value of the number of prestin molecules in each IMP was statistically different from a known value (such as 3 or 4, which represents trimer or tetramer for protein oligomerization). $P < 0.05$ was considered to be statistically significant.

## RESULTS

### Overall outer hair cell shape and nonlinear capacitance

Normal OHCs have cylindrical cell bodies. The OHCs isolated from either the heterozygous or homozygous prestin-null mice appeared to have no obvious morphological defects under the light microscope (Fig. 1a), except for a decrement in OHC lengths (Liberman et al. 2002). Electromotility was undetectable in prestin-null OHCs and significantly reduced in the heterozygotes (Liberman et al. 2002). OHC electromotility has an electrical signature, or a gating charge movement thought to arise from a redistribution of charged voltage sensors across the membrane. This charge movement imparts nonlinear, bell-shaped voltage dependence to the membrane capacitance (Ashmore 1989;Santos-Sacchi 1991). Measures of the gating currents associated with electromotility have been used in estimating the number of motor molecules (Santos-Sacchi 1991) in a manner similar to the one in which the density of ion channels in a membrane is estimated (Hille 2001). We measured nonlinear capacitance (NLC) from WT and prestin-deficient mice to determine whether the gating charge density was reduced. Examples of such measurements from representative OHCs are provided in figure 1b. Prestin-null OHCs exhibited no voltage-dependent NLC, indicating

that no prestin-associated gating charges were translocated during voltage stimulation. This is consistent with previous findings that prestin-null OHCs have no electromotility (Liberman et al. 2002). The WT and heterozygous mice both showed bell-shaped NLC-voltage relations. We computed six parameters by fitting the capacitance data from 23 WT and heterozygous 22 OHCs with the derivative of a first-order Boltzmann function (Santos-Sacchi 1991). The values of these parameters that include the maximum charge displacement ($Q_{max}$), the slope (α), the voltage at peak capacitance ($V_{1/2}$), the valence of charge movement ($z$), the NLC ($C_{non\text{-}lin}$), and the linear capacitance ($C_{lin}$) are presented in the figure caption of Fig. 1. While α, $z$, and $V_{1/2}$ values between the WT and heterozygous OHCs were not statistically different (p=0.7, 0.7, and 0.7, Student's unpaired t-test), the $Q_{max}$ and $C_{non\text{-}lin}$ were significantly different between the two groups (p<0.001 for both parameters).

In order to calculate the charge density, we measured the total surface area of the lateral membrane from OHCs where the NLC data were acquired. OHCs are cylindrical and its surface area can be calculated as: $A_s=\pi DL$, with D being the diameter, and L, the length of the cell. The length of the lateral membrane was measured from just below the cuticular plate to the plane of the lower end of the nucleus, whereas the cell's width (diameter) was measured by averaging the diameters measured in the midpoint of the cell and the nucleus area (inset, Fig. 1b). The reason to adopt such criteria is that the motor protein is not expressed in the ~ 1μm tight-adherens apical junctional belt (Nunes et al. 2006) and in the synaptic membrane below the nucleus (Belyantseva et al. 2000a). The average length and width of the lateral membrane portion were 16.6±1.7 and 6.2±0.1μm for the WT and 15.0±1.1 and 6.2±0.1μm for the heterozygous mice. Therefore, the total area of the lateral membrane containing prestin was 322±36 $\mu m^2$ for the WT and 291 ± 22 $\mu m^2$ for the heterozygous mice. The $z$-value for the WT and heterozygous OHCs was 0.79±0.12 and 0.78±0.12, respectively. The total elementary charge (calculated as $Q_{max}$ × 1C, 1C = 6.24 × $10^{18}$ elementary charges) was 6109 ± 1139 × $10^3$ and 4494 ± 995 × $10^3$ for the WT and heterozygous OHCs, respectively. The density of total elementary charge (calculated as total elementary charge divided by the total area of the lateral membrane) was 19.03 ± 3.34 × $10^3/\mu m^2$ and 15.43 ± 2.94 × $10^3/\mu m^2$ for the WT and heterozygous mice. The reduction of total elementary charge density between the WT and heterozygous mice was statistically significant (p<0.001).

## Prestin expression levels and IMP density

We used immunogold electron microscopy to probe prestin expression levels in the OHCs. Immunogold labeling using the affinity purified antibody raised against the C-terminus peptide sequence of prestin showed localization of prestin at the lateral plasma membrane, matching the localization shown previously with immunofluorescence (Belyantseva et al. 2000a). The calculated number of gold particles per micron cross section of membrane was 14.4 ± 2.8 (n = 30) for the WT and 11.1 ± 2.8 (n = 30) for the heterozygote (Fig. 2a,b). The reduction in of gold particles between WT and heterozygous OHCs was statistically different (p<0.01). No gold particles were observed along the lateral plasma membrane of the prestin-null OHCs (Fig. 2c). This is consistent with lack of prestin expression demonstrated in the previous studies (Liberman et al., 2002; Dallos et al., 2008).

To examine the changes in intramembrane protein particle (IMPs) distribution and density in the membrane where prestin expression is reduced or absent, we examined freeze-fracture replicas (Fig. 2d–f). Freeze-fracture images of the protoplasmic fracture face of the lateral plasma membrane of the WT OHCs showed the characteristic high density of predominantly large IMPs. The estimated density of IMPs in the WT was 5.6 ± 0.80 × $10^3/\mu m^2$ (number of membrane regions examined = n=15; number of cells examined = nc=4). The protoplasmic fracture face of the lateral plasma membrane of the heterozygous OHCs also contained high

density IMPs. However, the membrane showed an uneven density distribution, with areas containing high density and areas with low (or normal) density of IMPs (Fig. 2e). We randomly selected large areas and calculated the IMP density. The estimated average IMP density for the heterozygote was $5.5 \pm 1.5 \times 10^3/\mu m^2$ (n=15; nc=4). The protoplasmic fracture face of the lateral plasma membrane of the homozygous OHC lacked the high-density distribution of large IMPs and exhibited a random distribution of IMPs similar to that seen in the plasma membrane of other cells such as Deiters'cells (as shown in figure 3e). The estimated IMP densities for the prestin-null OHC lateral membrane and for the Deiters' plasma membrane were $2.9 \pm 0.38 \times 10^3/\mu m^2$ (n =12; nc=4) and $3.1 \pm 0.59 \times 10^3$ (n=10; nc=4), respectively.

## Comparison of charge density with IMP density

An important question regarding prestin function is the degree of oligomerization of the protein in OHCs. Prestin oligomerization has been evaluated by biochemical techniques (Zheng et al. 2006). We analyzed oligomerization by comparing the charge density of prestin obtained from the NLC measurement and the density of IMPs obtained from the freeze fracture data. We questioned how many prestin molecules were contained in each IMP. The number of prestin molecules in each IMP can be estimated based on prestin charge density and the average IMP density. In figure 4b, we presented the distribution pattern of number of prestin molecules calculated based on the charge density averaged for 23 WT and 22 heterozygous OHCs and the average IMP density presented above. The distribution pattern shows that a large proportion of WT OHCs average 3.5 to 4.5 prestin molecules per IMP. In heterozygous OHCs, however, each IMP contained fewer prestin molecules. The majority of them have 2.5 to 3.5 molecules per particle. In a typical measurement, the charge density can be underestimated due to damage and possible detrimental effect of enzymatic digestion during isolation. In order to minimize this potential underestimation, we selected 10 OHCs from each group that had higher charge density for our calculation from 23 WT and 22 heterozygous OHCs. The charge density for this selected group of measurements was $22.14 \pm 2.00 \times 10^3$ elementary charges per $\mu m^2$ for the WT. Based on the count of the average IMP density of $5.6 \pm 0.80 \times 10^3/\mu m^2$ from the freeze-fracture images, we calculated the number of prestin molecules in each IMP by dividing the total charge density by IMP density from the freeze-fracture count. The mean value of the number of prestin molecules in each IMP in the WT was estimated to be $3.92 \pm 0.35$. This value was not statistically different from the mean value of 4 (One-sample *t* test, $P = 0.49$) for a tetramer, suggesting that each IMP in the WT OHC contains four prestin molecules. In the heterozygote, the charge density for the selected group of the 10 highest values measured was $18.08 \pm 2.8 \times 10^3$ elementary charges per square micron. Based on the count of the average IMP density of $5.5 \pm 1.5 \times 10^3/\mu m^2$ obtained from the freeze-fracture for heterozygous OHCs, the mean value of the number of prestin molecules in each IMP was estimated to be $3.26 \pm 0.5$. This value was statistically different from the mean value of 4 (one-sample *t* test, $P$=0.001) for a tetramer, suggesting that some IMPs in the heterozygotes could be trimers or dimers.

## Intramembrane particle size and density

To evaluate the contribution of prestin to the density and size of IMPs in the lateral plasma membrane of OHCs, we compared the distribution of IMP diameter measurements for the three different prestin genotypes, as well as the IMP distribution in the lateral plasma membrane of Deiters' cell. Diameter measurements made in high magnification images (Fig. 3a–d) are shown as distribution plots in figure 4a. The average values for the diameter measurements were: WT = 11.9±1.6 nm (n=300); heterozygote = 9.4± 2.0 nm (n=300); homozygote = 7.2 ± 2.0 nm (n=300); Deiters' cell membrane = 7.7 ± 1.9 nm (n=300). It is apparent from figure 4a that majority of the IMPs in WT OHCs have a diameter between 10

and 13.5 nm. Particles with diameter less than 7.2 nm only account for less than 5% of the total population. In contrast, the majority of the IMPs in prestin-null OHCs are centered in the diameter range between 5 and 7.5 nm. We compared the size (diameter) distribution of the putative prestin IMPs to that of the gap junction IMPs (connexons), which are abundant in the supporting cells of the organ of Corti, and could be easily visualized in the same freeze-fracture replicas used to analyze the OHC lateral plasma membrane (Fig. 4c–e). The diameter of individual connexons, which correspond to hexamers of connexin, measured in their native condition by atomic force microscopy (AFM) is ~6 nm (Muller et al. 2002). Like the putative prestin IMPs, the gap junction IMPs also partition with the protoplasmic face of the membrane during freeze-fracture. The diameter of the gap junction IMPs in our freeze-fracture replicas was 8.4 ± 0.9 nm. The larger diameter of the connexons measured in our replicas as compared to the AFM measurements, was probably due to a combination of plastic deformation that follows the splitting of the membrane in two halves during the freeze-fracture procedure and the metal deposition during replication with platinum/carbon. The measured diameter for the OHC membrane IMPs in our freeze-fracture replicas was 11.92 ± 1.6 nm for the WT and 9.4 ± 2.0 nm for the heterozygote. These values are larger than the diameter for the connexon and show a more heterogeneous size distribution (Fig. 4e). While some IMPs (especially the smaller sized IMPs) in the WT OHC lateral plasma membrane may not contain prestin, the large majority of larger IMPs are likely to be made of prestin. Still, we cannot identify based only on shape which ones are unequivocally prestin IMPs. Gap junction IMPs typically leave complementary pits (or “empty holes”) in the exoplasmic fracture face. The exoplasmic fracture face of the WT OHC lateral plasma membrane (Fig. 4f) shows randomly distributed IMPs and scalloped texture, presumably due to the pits left by the proteins that partitioned with the protoplasmic half of the membrane. In summary, lateral plasma membrane of WT OHCs contained a high density of large (~12 nm) IMPs that are likely to correspond to prestin oligomers. These putative prestin IMPs are densely packed, but this does not exclude the existence of other proteins as evident from the presence of smaller particles as well as IMPs that partition with the exoplasmic fracture face. The lateral plasma membrane of the heterozygous OHCs contains virtually the same density of IMPs as the WT but the average diameter is reduced, suggesting the possibility that the number of prestin proteins per IMPs has changed.

## Cortical cytoskeletal lattice is absent in prestin null mice

The OHC lateral wall consists of the plasma membrane, the cortical lattice, and the subsurface cisternae. Since prestin constitutes a significant proportion of the proteins of the plasma membrane and the membrane is anchored to the cortical lattice by cross bridges (see diagram in Fig. 5c), or 'pillar' structures (Holley et al. 1992), we inquired whether alteration in prestin density or the absence of prestin affects the cortical lattice and the mechanical properties of OHCs. Conventional thin section electron microscopy of the prestin-null OHCs showed the characteristic organization of a typical OHC with the normal appearance of stereocilia, cuticular plate, tight-adherens junction (Nunes et al. 2006), subsurface cisternae underlying the lateral plasma membrane, attachment to the Deiters’ cell, and efferent synapses (Fig. 5). Thin sections grazing or tangent to the curved surface of the lateral wall of the WT and heterozygous OHCs (Fig. 5c–e) consistently showed the cortical actin-spectrin cytoskeletal lattice between the lateral plasma membrane and the underlying subsurface cisterna, identified as parallel actin filaments and periodic puncta. However, in the prestin-null mice (n=4), despite the normal overall appearance of the OHCs (more than 10 cells per animal) and the presence of the lateral subsurface cisternae, we could not observe the distinct parallel filaments and periodic puncta characteristic of the cortical cytoskeletal lattice (Fig. 5f).

### Reduction of axial stiffness in prestin deficient OHCs

Under the influence of the cell's turgor pressure, the plasma membrane and the cortical lattice contribute to the global axial stiffness of OHCs (Hallworth 1995; Holley and Ashmore 1988; Iwasa and Adachi 1997; Ulfendahl et al. 1998; Zenner et al. 1992). We measured axial stiffness of OHCs from the WT and prestin-deficient mice to determine whether alteration in prestin expression and cortical lattice would affect the axial stiffness of OHCs. The stiffness of prestin-null OHCs has been measured using the micro chamber technique (Dallos et al., 2008). However, isolated OHCs are normally depolarized and their resting membrane potential can vary significantly. Because membrane potential can affect axial stiffness (He and Dallos, 2000), we measured and compared axial stiffness from three populations of the OHCs at the same membrane potential (−70 mV) under the voltage-clamp condition. We only selected OHCs with cell length between 18 and 20 μm for comparison because the axial stiffness also depends on the cell length (Hallworth 1995). Examples of the responses obtained from the three phenotypes are presented in figure 6a. In figure 6a, the responses of the loaded fiber (black lines) are superimposed on those of the unloaded-fiber motion (gray lines). Since the cell served as a mechanical load against the vibrating probe, the change in magnitude with and without load would reflect the stiffness of the cells. A cell with greater stiffness would result in greater reduction in magnitude of the loaded fiber motion. With the known stiffness of the fibers, we computed the stiffness of the OHCs. The axial stiffness was 2.9±0.4 (n=9), 2.5±0.4 (n=9), and 1.1±0.2 (n=8) mN/m, respectively, for the WT, heterozygous, and homozygous OHCs. That translates to a stiffness reduction of 14% and 62% for the heterozygous and homozygous OHCs, with reference to their WT counterpart. The reduction of stiffness in heterozygous and homozygous OHCs was statistically significant comparing with the WT OHCs (p=0.03 and 0.001). The stiffness of homozygous OHCs was also significantly less than that of the heterozygous OHCs (p=0.001).

### Loss of voltage-dependent stiffness and piezoelectric property in prestin deficient OHCs

Mechanical stretch or stress of OHC membrane can induce a rapid charge movement resulting from the reversal of the electromechanical transduction process in OHCs (Dong et al. 2000; Gale and Ashmore 1994). The charge movement reflects the piezoelectric property of OHCs. We measured the compression-evoked gating charge displacement in the prestin-deficient OHCs to determine whether such piezoelectricity of OHCs was an inherent characteristic of prestin. OHCs were voltage-clamped at −70 mV. The piezoelectric current was measured in the same experiments when the axial stiffness of the cells was measured. Figure 6b shows current responses recorded from three representative OHCs. As shown, compression of the cells evoked an outward current in both WT and heterozygous OHCs. However, the compression-evoked response was not observed in any of the 8 prestin-null OHCs. This suggests that the piezoelectric current is indeed associated with prestin function. We compared the piezoelectric efficiency of OHCs from WT and heterozygous OHCs by normalizing the amplitude of piezoelectric current with the magnitude of cell compression. The mean values were 0.176±0.022 pA/nm (n=8) and 0.147±0.019 pA/nm (n=8) for the WT and heterozygous OHCs, respectively. Student's T-test showed that these values were statistically significant (p=0.016). The piezoelectric efficiency of heterozygous OHCs was ~17% less than that of WT OHCs.

OHCs exhibit a voltage-dependent stiffness (He and Dallos 1999), which disappears after somatic motility is blocked (He et al. 2003). We measured voltage-dependent stiffness in WT and prestin-null OHCs to determine whether absence of prestin also abolished voltage-dependent stiffness change. Two voltage steps (50 mV in step size) were used to evoke motility and stiffness changes in the depolarizing and hyperpolarizing directions from the holding potential of −70 mV. Five cells each from WT and prestin-null mice were examined

for voltage-dependent stiffness changes under whole-cell voltage-clamp condition. Motility was first measured without loading the cell with a fiber. After motility was measured, a glass fiber with known stiffness was loaded onto the surface of the cuticular plate of the cell. The fiber was driven sinusoidally at 100 Hz, while the OHC was electrically stimulated with 50-mV voltage steps around the holding potential of −70 mV. During the steps, the amplitude of the 100-Hz fiber-motion was altered (Fig. 7). Hyperpolarization produced cell elongation and a decrease in the amplitude of fiber motion. Conversely, depolarization of the cell produced contraction and an increase in fiber amplitude (Fig. 7, left panels). The alteration in the magnitude of fiber-driven response reflected the voltage-dependent stiffness change; hyperpolarization increased the axial stiffness of the cell, while depolarization decreased the stiffness. For the prestin-null OHCs, no motility was observed. Importantly, when motility was absent, the voltage-dependent stiffness change also disappeared. This is reflected by the lack of modulation of the magnitude of fiber-driven motion during depolarization and hyperpolarization of the cell (right panels in Fig. 7).

## DISCUSSION

Outer hair cell electromotility is believed to be the result of the concerted action of a large number of independent molecular motors closely associated within the cell's basolateral membrane. Morphological studies show that densely packed IMPs cover the lateral plasma membrane (Gulley and Reese 1977) where electromotility is generated (Kalinec et al. 1992). A general hypothesis is that some or the majority of the particles are the molecular motor prestin (Koppl et al. 2004). Here we provided evidence that the majority of these particles are indeed prestin. We showed that when prestin was absent, the density of IMPs was significantly reduced and the replicas of the lateral membrane showed IMP distribution and density comparable to other membranes that do not contain prestin. Correspondingly, we showed that NLC, motility, and piezoelectric current all disappeared when prestin was absent in the membrane. The correlation between significant reduction of IMPs and loss of NLC and motility strongly suggests that the majority of the IMPs are indeed formed by prestin. The correlation between absence of prestin and loss of motility, voltage-dependent stiffness, and piezoelectricity in prestin-null OHCs further confirms the essential role of prestin for these unique properties of OHCs.

The membrane of WT OHCs is dominated by IMPs with diameter between 9 and 13 nm. The particles with size of less than 8 nm make up less than 5% of the total IMPs seen in the membrane (Fig. 4a). It appears that the expression of prestin partially precludes the presence of other proteins due to the high-density packing. In prestin-null OHCs, the majority of the IMPs have a particle diameter of less than 7.5 nm. Although it is hard to determine to what extent the particles in the prestin-null membranes are actually present in the WT, it is likely that many membrane proteins are repopulating the lateral plasma membrane in place of the missing prestin in the prestin-null OHCs. The fact that the OHC lateral membrane can lose ~90 % of its proteins and maintain its structural integrity mirrors the conditions during development of electromotilty when, within a few days, the OHC lateral membrane incorporates and densely packs a remarkable amount of prestin molecules(Souter et al. 1995).

In heterozygous OHCs, the prestin density is reduced as demonstrated in NLC measurements and in immunogold labeling. Mechanical stress-induced piezoelectric current is also reduced. All these are consistent with the reduction of OHC motility reported in the previous study (Liberman et al. 2002). Interestingly, in heterozygous OHCs the distribution of IMPs is not uniform. The membrane exhibits patches of IMP-rich and IMP-poor regions, suggesting that prestin has a natural tendency to aggregate into dense packing. This tendency to form aggregates before it is fully confluent is also observed during development

when prestin expression levels increase progressively (data not shown). An example of clustering of a particular type of membrane protein and exclusion of other membrane proteins from large expanses of membrane area occurs during formation of gap junctions (Kachar and Reese 1985).

The predicted membrane topology and molecular mass of a single prestin molecule (744 amino acids with a molecular mass of ~81.4 kDa) appear inadequate to account for the size of IMPs. It is well known that ion channels and transporters in the membrane form oligomers and that the nature of oligomerization influences the properties of gating and selectivity. For example, some recent studies using biochemical and electron microscopic techniques suggest that prestin likely is comprised of four homologous subunits (Mio et al. 2008; Pasqualetto et al. 2008; Zheng et al. 2000), while another study suggests that prestin likely forms dimers in the membrane (Detro-Dassen et al., 2008). Therefore, the oligomeric structure of prestin remained controversial. We examined prestin oligomerization by a different approach. We estimated how many prestin molecules are contained in each IMP by comparing the prestin-related elementary charges per square micron with the average IMP density. The mean charge density ($22.1 \times 10^3$ elementary charges/$\mu m^2$) measured from WT OHCs was approximately four times the average density of IMPs ($5.6 \times 10^3$ IMPs/$\mu m^2$), suggesting that each IMP contains four prestin molecules. Santos-Sacchi et al (Santos-Sacchi et al. 1998) showed that the IMP density is not related with cochlear locations. The average density of IMPs in gerbil OHCs is about 5686 particles/$\mu m^2$ (Koppl et al. 2004) similar to the average IMP density found in our study. We used the average IMP density of $5.6 \times 10^3$ IMPs/$\mu m^2$ for the calculation. This requires some explanation since the membrane of prestin-null OHCs still contains the IMPs similar to the membrane of other cells. Although the average density of ~$2.9 \times 10^3$ particles/$\mu m^2$ is present in the prestin-null OHCs, the size of the majority of particles is ~7.2 nm, which is significantly smaller than the average size of ~11.9-nm particles seen in the WT OHCs (Fig. 3). Although the nature of these small IMPs is unknown, they apparently are not prestin. The membrane of WT OHCs also contains some small IMPs (about 8 nm in diameter); they make up less than 5% of the total IMPs seen in the membrane (Fig. 4a). Ninety five percent of the IMPs in the WT OHCs have a diameter larger than 9 nm. It is conceivable that the majority of IMPs seen in the membrane are prestin. Therefore, it is reasonable to use their average density ($5.6 \times 10^3$ IMPs/$\mu m^2$) for the calculation. It is conceivable that reduction in the IMP average diameter in the heterozygous (Fig. 3) may reflect a reduction in number of prestin molecules in each IMP. If we use the particle density of $5.5 \times 10^3$ IMPs/$\mu m^2$ for heterozygous OHCs to estimate how many prestin molecules in one particle, the ratio (between mean charge density and the average density of IMPs) is ~3, suggesting that some of the IMPs could be trimers or dimers. If this were indeed the case, it would then suggest that each prestin molecule could function normally and independently, regardless of whether prestin exists as tetramers or other oligomers in the membrane. We recognize that, in the membrane of heterozygous OHCs, the distribution of IMPs is not uniform. The membrane exhibits patches of IMP-rich and IMP-poor regions. This might cause overestimation of the area containing elementary charges and therefore, underestimation of the elementary charge density. Since the size and number of these areas are difficult to measure, it is hard to determine how much they would influence the calculation of charge density. We should point out that dimers, trimers, and tetramers are among all those seen in the prestin-expressing cell lines and in native OHCs using biochemical methods (Detro-Dassen et al. 2008; Zheng et al. 2006). It is possible that these high-order oligomers (such as trimer and tetramer) can co-exist and are functional.

Since prestin was discovered, a great deal of effort has been made to understand whether somatic motility is responsible for cochlear amplification (Dallos et al. 2008; Gao et al. 2007; Liberman et al. 2002; Mellado Lagarde et al. 2008). What is still not well understood

is how OHC stiffness and length changes emerge from prestin function and whether stiffness and length changes are related at the structural or molecular level. Ultimately, what is still missing is a clear structural framework for the lateral wall and information on how prestin molecules interact with each other and with the underlying cortical cytoskeleton. The electromotility mechanism is unique in its basic organization and is fundamentally different from other well-studied motile systems (Frolenkov et al. 1998a). The mechanisms of force generation are membrane-based but the underlying cytoskeleton is an integral part of the force translation into the cell shape and stiffness changes that characterize the electromotility. The detailed mechanism of force production and propagation depends on a detailed structural framework, in particular the identity of the pillar elements that connect the underlying cytoskeleton to the membrane. The fact that prestin is required to form or retain the organized actin cytoskeletal lattice suggests that the membrane and the cortical lattice are structurally and functionally interdependent.

The present study shows that the average axial stiffness of the prestin-null OHCs is reduced by as much as 62% of that of the WT OHCs. The reduction is consistent with that reported in a previous study (Dallos et al. 2008). This reduction is greater than the stiffness reduction seen in the previous study (He et al. 2003), which showed that the average axial stiffness is reduced by about ~50% when the prestin-based motility is blocked by removal of intracellular $Cl^-$. There is also a significant reduction of stiffness in the heterozygous OHCs (Fig. 6), consistent with the reduction of prestin charge density in the membrane (Fig. 1 and Fig. 2). It is conceivable that a significant portion of the stiffness reduction of the prestin-null OHCs is the result of loss of prestin in the lateral wall. The disruption of organization and orientation of actin filaments and pillar proteins in the cortical lattice may also contribute to the reduction of overall stiffness. Our results suggest that the plasma membrane, which contains the closely packed motor protein, is a significant contributor to the stiffness of the OHC's composite lateral wall. The possibility that the plasma membrane is a significant contributor to the OHC lateral wall's longitudinal or axial stiffness is quite intriguing. In thin section electron microscopy, the plasma membrane appears as just a very slim line contributing to the overall structure of the lateral wall, which also contains the cortical lattice and in some hair cells also contains multiple parallel cisternae. However, this apparent "thin-shell structure" is consistent with the conclusions of Holley and Ashmore (Holley and Ashmore 1988), who suggest that most of the lateral wall stiffness is inherent to the plasma membrane.

By measuring the amplitude of driven vibrations of a fiber that was loaded by an isolated OHC while the cell was electrically stimulated under whole-cell voltage-clamp, it was shown that the amplitude of fiber motion was significantly modulated during the contraction—elongation cycle of the cell. The finding is interpreted as a voltage-dependent axial stiffness change of OHCs (Frolenkov et al. 1998b; He and Dallos 1999). It is noted that Hallworth (2007) did not see any voltage-dependent stiffness in the basal turn OHCs from the guinea pig. However, the voltage-dependent stiffness and voltage-dependent cell length are clearly related; several such relationships were revealed in a previous study (He and Dallos 2000). The most suggestive relationship is the same dependence on prestin, as shown in this study: absence of prestin abolishes both motility and voltage-dependent stiffness (Fig. 7). The general covariance of stiffness and length changes indicates that they may arise from a common mechanism, the motor protein.

It is interesting to note that NLC, pizeoelectrical current, and passive stiffness were reduced in heterozygous OHCs. However, the differences in all these measurements did not reach the 50% reduction that one would expect from one functional allele in the heterozygous as opposed to two functional alleles in the WT mice. Cheatham et al (2005) (Cheatham et al. 2005) also showed that while one copy of prestin generates about half the mRNA as

revealed by real-time PCR, the level of prestin protein (determined by western blot) in the heterozygous OHC is reduced by only 10–12 %. This is consistent with our functional measurements of prestin. The nature of this discrepancy is unknown. It is possible that prestin expression is regulated post-transcription and OHCs compensate for the deleted prestin gene in the heterozygous mice, thereby minimizing deleterious effects on peripheral auditory function.

## Acknowledgments

This work was supported by NIDCD, DIR, NIH (to B.K.) and NIH grants DC 004696 to D.H., DC 06471 to J.Z.

## References

Adler HJ, Belyantseva IA, Merritt RC Jr, Frolenkov GI, Dougherty GW, Kachar B. Expression of prestin, a membrane motor protein, in the mammalian auditory and vestibular periphery. Hear Res. 2003; 184(1–2):27–40. [PubMed: 14553901]

Ashmore, JF. Transducer motor coupling in cochlear outer hair cells. Kemp, D.; Wilson, JP., editors. New York: Plenum Press; 1989.

Belyantseva IA, Adler HJ, Curi R, Frolenkov GI, Kachar B. Expression and localization of prestin and the sugar transporter GLUT-5 during development of electromotility in cochlear outer hair cells. J Neurosci. 2000a; 20(24):RC116. [PubMed: 11125015]

Belyantseva IA, Frolenkov GI, Wade JB, Mammano F, Kachar B. Water permeability of cochlear outer hair cells: characterization and relationship to electromotility. J Neurosci. 2000b; 20(24): 8996–9003. [PubMed: 11124975]

Brownell WE, Bader CR, Bertrand D, de Ribaupierre Y. Evoked mechanical responses of isolated cochlear outer hair cells. Science. 1985; 227(4683):194–196. [PubMed: 3966153]

Brownell, WE.; Kachar, B. Outer hair cell motility: a possible electrokinetic mechanism. Allen, JB., editor. New York: Springer-Verlag; 1985.

Cheatham MA, Zheng J, Huynh KH, Du GG, Gao J, Zuo J, Navarrete E, Dallos P. Cochlear function in mice with only one copy of the prestin gene. J Physiol. 2005; 569(Pt 1):229–241. [PubMed: 16166160]

Dallos P, He DZ. Two models of outer hair cell stiffness and motility. J Assoc Res Otolaryngol. 2000; 1(4):283–291. [PubMed: 11547808]

Dallos P, Wu X, Cheatham MA, Gao J, Zheng J, Anderson CT, Jia S, Wang X, Cheng WH, Sengupta S, et al. Prestin-based outer hair cell motility is necessary for mammalian cochlear amplification. Neuron. 2008; 58(3):333–339. [PubMed: 18466744]

Detro-Dassen S, Schanzler M, Lauks H, Martin I, zu Berstenhorst SM, Nothmann D, Torres-Salazar D, Hidalgo P, Schmalzing G, Fahlke C. Conserved dimeric subunit stoichiometry of SLC26 multifunctional anion exchangers. J Biol Chem. 2008; 283(7):4177–4188. [PubMed: 18073211]

Dong X, Ehrenstein D, Iwasa KH. Fluctuation of motor charge in the lateral membrane of the cochlear outer hair cell. Biophys J. 2000; 79(4):1876–1882. [PubMed: 11023893]

Dumont RA, Lins U, Filoteo AG, Penniston JT, Kachar B, Gillespie PG. Plasma membrane Ca2+ATPase isoform 2a is the PMCA of hair bundles. J Neurosci. 2001; 21(14):5066–5078. [PubMed: 11438582]

Frolenkov GI, Atzori M, Kalinec F, Mammano F, Kachar B. The membrane-based mechanism of cell motility in cochlear outer hair cells. Mol Biol Cell. 1998a; 9(8):1961–1968. [PubMed: 9693359]

Frolenkov GI, Belyantseva IA, Kachar B. Electromotility influences the axial stiffness of the outer hair cells. 1998b:254.

Gale JE, Ashmore JF. Charge displacement induced by rapid stretch in the basolateral membrane of the guinea-pig outer hair cell. Proc Biol Sci. 1994; 255(1344):243–249. [PubMed: 8022840]

Gao J, Wang X, Wu X, Aguinaga S, Huynh K, Jia S, Matsuda K, Patel M, Zheng J, Cheatham M, et al. Prestin-based outer hair cell electromotility in knockin mice does not appear to adjust the operating point of a cilia-based amplifier. Proc Natl Acad Sci U S A. 2007; 104(30):12542–12547. [PubMed: 17640919]

Geleoc GS, Casalotti SO, Forge A, Ashmore JF. A sugar transporter as a candidate for the outer hair cell motor. Nat Neurosci. 1999; 2(8):713–719. [PubMed: 10412060]

Goldstein AJ, Mizukoshi O. Separation of the organ of Corti into its component cells. Ann Otol Rhinol Laryngol. 1967; 76(2):414–426. [PubMed: 5339231]

Gulley RL, Reese TS. Regional specialization of the hair cell plasmalemma in the organ of corti. Anat Rec. 1977; 189(1):109–123. [PubMed: 907202]

Hallworth R. Passive compliance and active force generation in the guinea pig outer hair cell. J Neurophysiol. 1995; 74(6):2319–2328. [PubMed: 8747194]

Hallworth R. Absence of voltage-dependent compliance in high-frequency cochlear outer hair cells. J Assoc Res Otolaryngol. 2007; 8(4):464–473. [PubMed: 17934775]

He DZ, Dallos P. Somatic stiffness of cochlear outer hair cells is voltage-dependent. Proc Natl Acad Sci U S A. 1999; 96(14):8223–8228. [PubMed: 10393976]

He DZ, Dallos P. Properties of voltage-dependent somatic stiffness of cochlear outer hair cells. J Assoc Res Otolaryngol. 2000; 1(1):64–81. [PubMed: 11548238]

He DZ, Evans BN, Dallos P. First appearance and development of electromotility in neonatal gerbil outer hair cells. Hear Res. 1994; 78(1):77–90. [PubMed: 7961180]

He DZ, Jia S, Dallos P. Prestin and the dynamic stiffness of cochlear outer hair cells. J Neurosci. 2003; 23(27):9089–9096. [PubMed: 14534242]

Hille, B. Ionic channels of excitable membranes. Boston, Massachusetts: Sinauer Associates, Inc.; 2001.

Holley MC, Ashmore JF. A cytoskeletal spring in cochlear outer hair cells. Nature. 1988; 335(6191): 635–637. [PubMed: 3173482]

Holley MC, Kalinec F, Kachar B. Structure of the cortical cytoskeleton in mammalian outer hair cells. J Cell Sci. 1992; 102(Pt 3):569–580. [PubMed: 1506434]

Howard J, Ashmore JF. Stiffness of sensory hair bundles in the sacculus of the frog. Hear Res. 1986; 23(1):93–104. [PubMed: 3488306]

Iwasa KH. Effect of membrane motor on the axial stiffness of the cochlear outer hair cell. J Acoust Soc Am. 2000; 107(5 Pt 1):2764–2766. [PubMed: 10830400]

Iwasa KH, Adachi M. Force generation in the outer hair cell of the cochlea. Biophys J. 1997; 73(1): 546–555. [PubMed: 9199816]

Kachar B, Brownell WE, Altschuler R, Fex J. Electrokinetic shape changes of cochlear outer hair cells. Nature. 1986a; 322(6077):365–368. [PubMed: 3736662]

Kachar B, Christakis NA, Reese TS, Lane NJ. The intramembrane structure of septate junctions based on direct freezing. J Cell Sci. 1986b; 80:13–28. [PubMed: 3722279]

Kachar B, Reese TS. Rapid formation of gap-junction-like structures induced by glycerol. Anat Rec. 1985; 213(1):7–15. [PubMed: 4073563]

Kalinec F, Holley MC, Iwasa KH, Lim DJ, Kachar B. A membrane-based force generation mechanism in auditory sensory cells. Proc Natl Acad Sci U S A. 1992; 89(18):8671–8675. [PubMed: 1528879]

Koppl C, Forge A, Manley GA. Low density of membrane particles in auditory hair cells of lizards and birds suggests an absence of somatic motility. J Comp Neurol. 2004; 479(2):149–155. [PubMed: 15452826]

Liberman MC, Gao J, He DZ, Wu X, Jia S, Zuo J. Prestin is required for electromotility of the outer hair cell and for the cochlear amplifier. Nature. 2002; 419(6904):300–304. [PubMed: 12239568]

Mellado Lagarde MM, Drexl M, Lukashkina VA, Lukashkin AN, Russell IJ. Outer hair cell somatic, not hair bundle, motility is the basis of the cochlear amplifier. Nat Neurosci. 2008; 11(7):746–748. [PubMed: 18516034]

Mio K, Kubo Y, Ogura T, Yamamoto T, Arisaka F, Sato C. The motor protein prestin is a bullet-shaped molecule with inner cavities. J Biol Chem. 2008; 283(2):1137–1145. [PubMed: 17998209]

Muller DJ, Hand GM, Engel A, Sosinsky GE. Conformational changes in surface structures of isolated connexin 26 gap junctions. EMBO J. 2002; 21(14):3598–3607. [PubMed: 12110573]

Nunes FD, Lopez LN, Lin HW, Davies C, Azevedo RB, Gow A, Kachar B. Distinct subdomain organization and molecular composition of a tight junction with adherens junction features. J Cell Sci. 2006; 119(Pt 23):4819–4827. [PubMed: 17130295]

Oliver D, He DZ, Klocker N, Ludwig J, Schulte U, Waldegger S, Ruppersberg JP, Dallos P, Fakler B. Intracellular anions as the voltage sensor of prestin, the outer hair cell motor protein. Science. 2001; 292(5525):2340–2343. [PubMed: 11423665]

Pasqualetto E, Seydel A, Pellini A, Battistutta R. Expression, purification and characterisation of the C-terminal STAS domain of the SLC26 anion transporter prestin. Protein Expr Purif. 2008; 58(2): 249–256. [PubMed: 18226918]

Salles FT, Merritt RC Jr, Manor U, Dougherty GW, Sousa AD, Moore JE, Yengo CM, Dose AC, Kachar B. Myosin IIIa boosts elongation of stereocilia by transporting espin 1 to the plus ends of actin filaments. Nat Cell Biol. 2009; 11(4):443–450. [PubMed: 19287378]

Santos-Sacchi J. Reversible inhibition of voltage-dependent outer hair cell motility and capacitance. J Neurosci. 1991; 11(10):3096–3110. [PubMed: 1941076]

Santos-Sacchi J, Kakehata S, Kikuchi T, Katori Y, Takasaka T. Density of motility-related charge in the outer hair cell of the guinea pig is inversely related to best frequency. Neurosci Lett. 1998; 256(3):155–158. [PubMed: 9855363]

Santos-Sacchi J, Wu M, Kakehata S. Furosemide alters nonlinear capacitance in isolated outer hair cells. Hear Res. 2001; 159(1–2):69–73. [PubMed: 11520635]

Souter M, Nevill G, Forge A. Postnatal development of membrane specialisations of gerbil outer hair cells. Hear Res. 1995; 91(1–2):43–62. [PubMed: 8647724]

Ulfendahl M, Chan E, McConnaughey WB, Prost-Domasky S, Elson EL. Axial and transverse stiffness measures of cochlear outer hair cells suggest a common mechanical basis. Pflugers Arch. 1998; 436(1):9–15. [PubMed: 9560441]

Zenner HP, Gitter AH, Rudert M, Ernst A. Stiffness, compliance, elasticity and force generation of outer hair cells. Acta Otolaryngol. 1992; 112(2):248–253. [PubMed: 1604988]

Zenner HP, Zimmermann U, Schmitt U. Reversible contraction of isolated mammalian cochlear hair cells. Hear Res. 1985; 18(2):127–133. [PubMed: 2995297]

Zheng J, Du GG, Anderson CT, Keller JP, Orem A, Dallos P, Cheatham M. Analysis of the oligomeric structure of the motor protein prestin. J Biol Chem. 2006; 281(29):19916–19924. [PubMed: 16682411]

Zheng J, Shen W, He DZ, Long KB, Madison LD, Dallos P. Prestin is the motor protein of cochlear outer hair cells. Nature. 2000; 405(6783):149–155. [PubMed: 10821263]

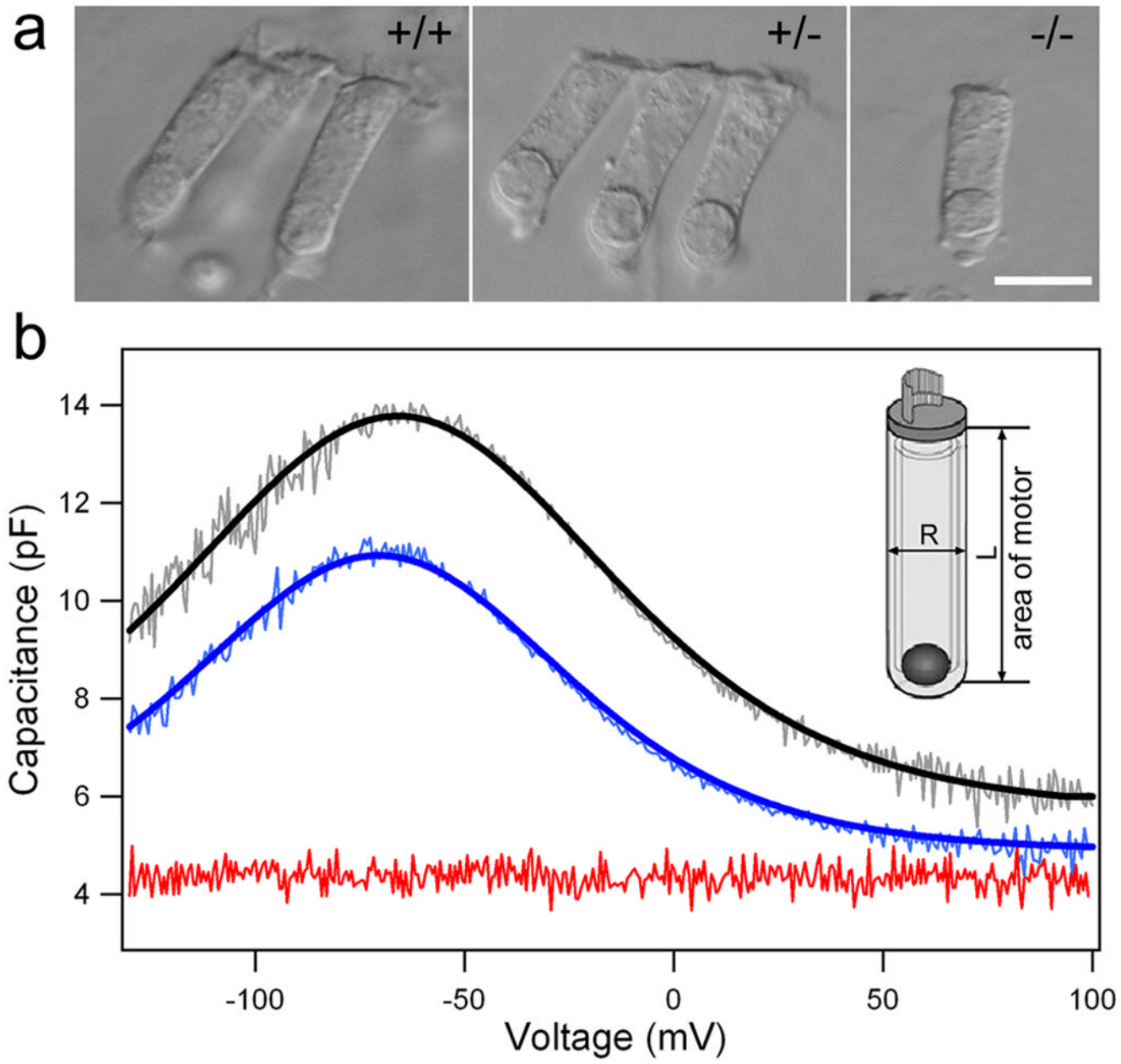


**Figure 1.**

Nonlinear capacitance (NLC) and 'gating' charge density measured from OHCs isolated from WT (+/+), heterozygous (+/−), and prestin-null (−/−) mice. (**a**) Images of isolated OHCs from the three genotypes. (**b**) Examples of the NLC measured from the three populations of OHCs. The NLC (lighter color lines) was fit with a two-state Boltzmann function (heavy lines). The NLC is color-coded; WT in black, heterozygous in blue, and prestin-null in red. The 6 parameters obtained from these cells are: $Q_{max}$ 978.9±182.6 fC, α 31.1±4.9 $mV^{-1}$, z 0.79±0.12, $V_{1/2}$ −65.2±29.4 mV, $C_{non\text{-}lin}$ 7.9±1.6 pF, $C_{lin}$ 5.69±0.83 pF (for +/+, n=23); $Q_{max}$ 720.1±159.6 fC, α 30.5±4.9 $mV^{-1}$, z 0.78±0.12, $V_{1/2}$ −68.9±33.9 mV, $C_{non\text{-}lin}$ 5.9±0.86 pF, $C_{lin}$ 5.39±0.55 pF (for +/−, n=22). The linear capacitance ($C_{lin}$) for homozygous OHCs is 4.8±0.34 pF (n=5). (b, inset) Schematic drawing of an OHC illustrates

how the total plasma membrane area containing prestin is calculated. Magnification bar in **a** equals 10 μm.

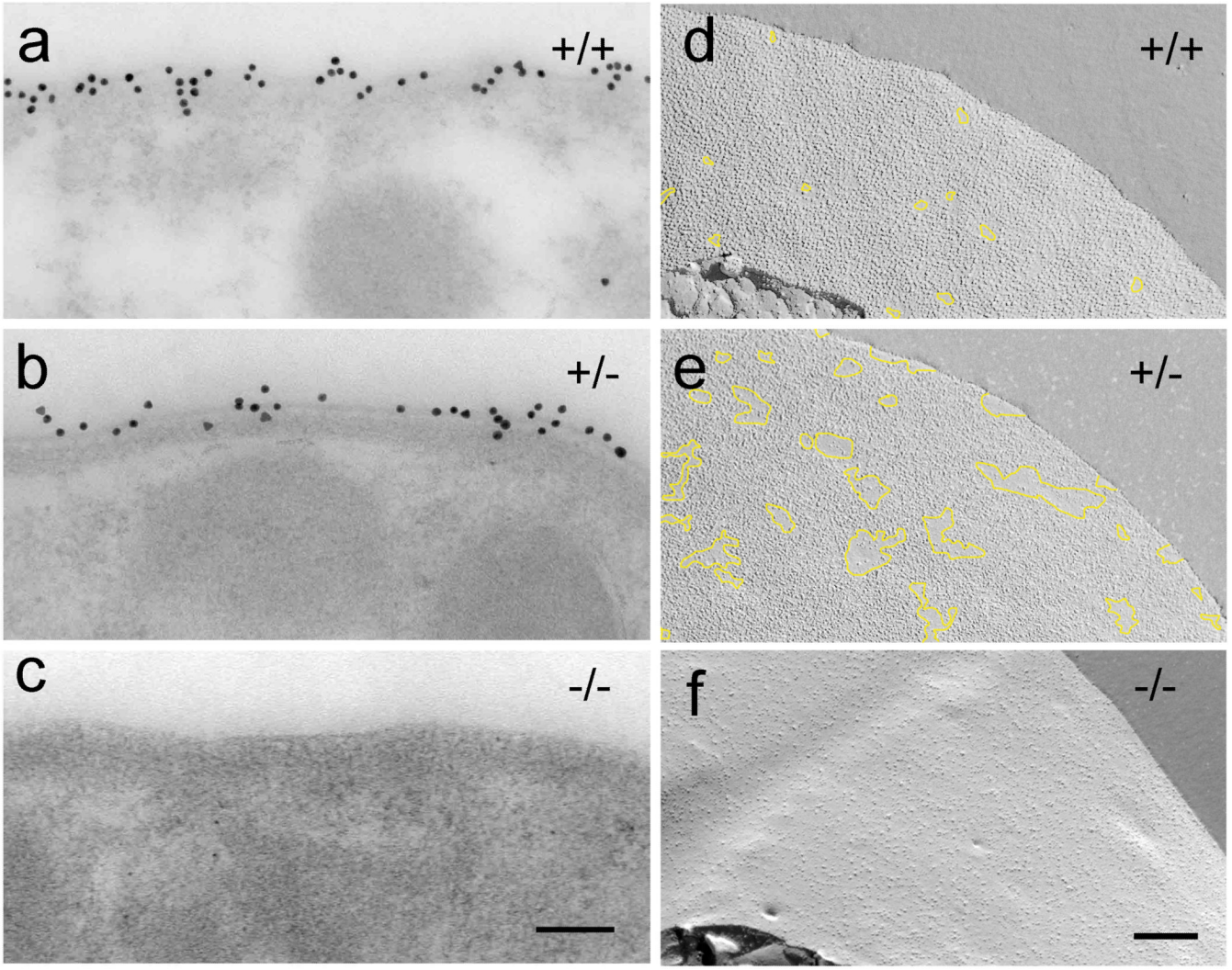


**Figure 2.**

Correlation between prestin expression levels and the presence of the high density of IMPs. (**a–c**) Prestin immunogold labeling of OHC lateral plasma membrane from +/+, +/−, and −/− mice. Prestin null OHCs show no immunogold labeling (**c**). Close up views of the protoplasmic freeze-fracture views of OHC lateral plasma membrane (**d–e**) from +/+, +/−, and −/− mice. In the WT, the protoplasmic fracture face characteristically shows a continuous high density of IMPs, where only very few and small areas devoid of IMPs can be found (delineated by the overlay trace in yellow). The protoplasmic fracture face of the lateral plasma membrane of the heterozygous OHC shows areas of high density and areas with normal density distribution of IMPs delineated by the overlay trace in yellow. The protoplasmic fracture face of the lateral plasma membrane of the prestin null OHCs lack the high-density distribution of IMPs (**f**). Magnification bars: 100 nm in (**a–c**) and 200 nm in (**d, f**)

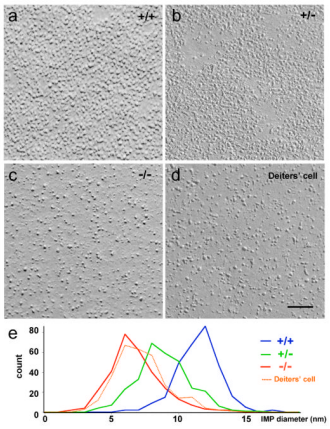


**Figure 3.**

Comparison of IMP size between wild type and prestin-deficient OHCs. High magnification images of the protoplasmic freeze-fracture face of the OHC lateral plasma membrane (a–c) from +/+,,+/−,and −/− mice as well as plasma membrane of Deiters'cell (**d**). Magnification bar equals 100 nm for **a–d**. (**e**) IMP diameter distribution for +/+, +/−, and −/− mice as well as plasma membrane of Deiters'cell.

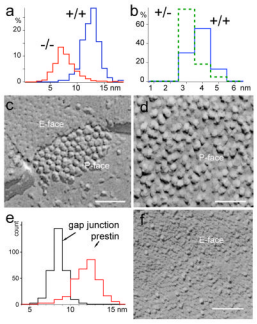


**Figure 4.**

Comparison of IMP size and shape between prestin and connexin oligomers. (**a**) Histogram of the diameters of IMPs in the OHC lateral membrane from the +/+ and −/− mice. (**b**) Estimated number of prestin molecules per IMP for the +/+ and +/− mice based on the ratio of non-linear capacitance and density of IMPs. (**c**) High magnification image of the freeze-fracture replica of a typical gap junction from an organ of Corti supporting cell. (**d**) High magnification image of the freeze-fracture replica of a typical region in the lateral plasma membrane from a WT OHC. In panel (**c**) both the exoplasmic (**E-face**) and protoplasmic (**P-face**) fracture faces can be visualized showing connexin IMPs in the **P-face** and complementary dimples in the **E-face**. (**e**) Histogram showing the distribution of IMP diameters for gap junction IMPs and for the IMPs from the prestin containing region of the lateral plasma membrane. (**f**) Exoplasmic fracture face of prestin containing region of the OHC lateral plasma membrane from WT mice shows IMPs dispersed on a scalloped surface likely resulting from the empty holes left when the IMPs were pulled out and portioned to the protoplasmic half of the membrane during freeze-fracture. Magnification bars equal: 50 nm in **c** and **d** and 100 nm in **f**.

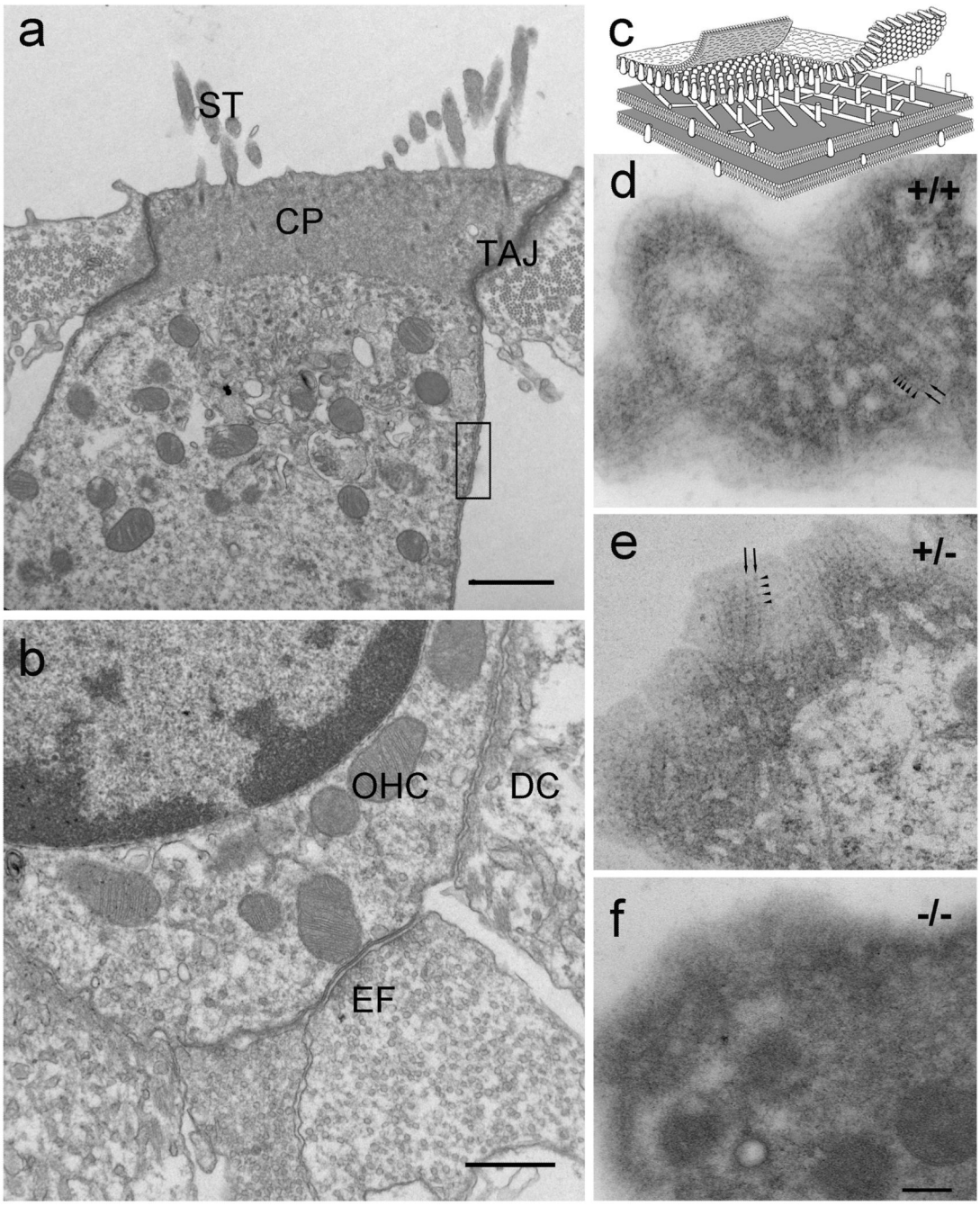


**Figure 5.**

Disruption of the cortical lattice in prestin-null OHCs. At the electron microscopic level the prestin-null OHC shows the characteristic organization of a typical OHC (**a, b**) with stereocilia (ST), cuticular plate (CP), tight-adherens junction (TAJ), subsurface cisternae underlying the lateral plasma membrane, attachment to the Deiters' cell (DC), and efferent synapses (EF). (*c*) Schematic diagram of a portion of the lateral wall of the OHC (equivalent to the region delineated by the rectangle in **a**) showing the cortical actin-spectrin cytoskeletal lattice between the lateral plasma membrane and the underlying subsurface cisterna. The parallel actin filaments (arrows) and the periodic puncta (arrowheads) characteristic of the cortical actin-spectrin lattice are clearly visualized in thin section

grazing or tangent to the curved surface of the OHC lateral wall (**d, e**) from the WT and hetereozygote but are absent in the prestin-null OHC (**f**). Magnification bars equal: 1 μm in **a**; 0.5 μm in **b**; and 200 nm in **d–f**.

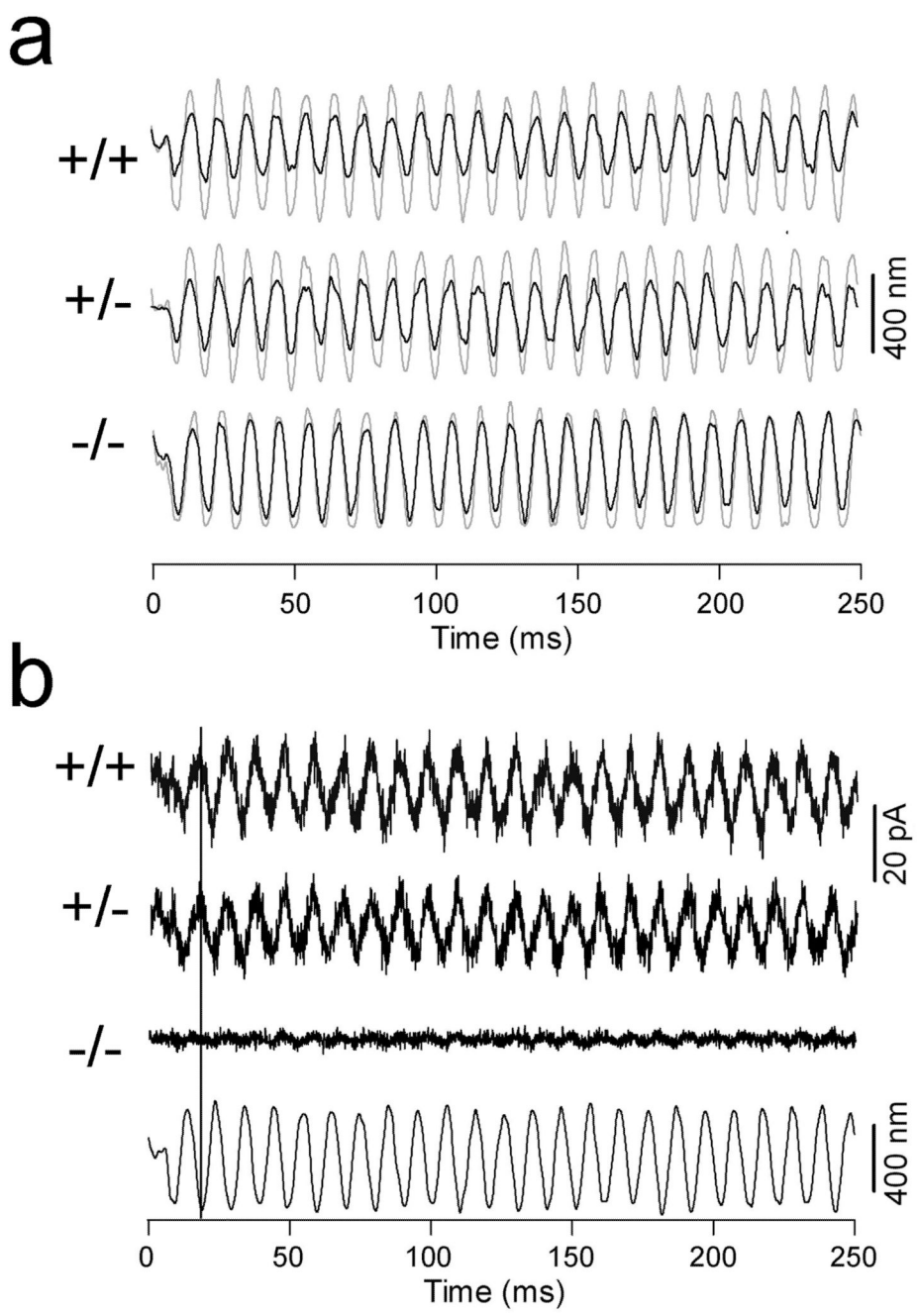


**Figure 6.**

Changes in axial stiffness and piezoelectric properties in prestin-deficient OHCs. (**a**) Measurement of passive axial stiffness. Examples of free-fiber (in light-color lines) and loaded-fiber motions (heavy lines) measured from the OHCs isolated from the cochleae of WT, heterozygous, and homozygous mice. The axial stiffness for the cells is 3.1 (+/+), 2.6 (+/−), and 0.9 (−/−) mN/m. (**b**) Examples of compression-evoked charge movement. Compression of the cell by a loaded fiber evoked an outward current in both +/+ and +/− OHCs. The current was absent in prestin-null OHCs. Bottom panel shows the waveform of the fiber motion. The black line indicates the direction of fiber motion (compression) and the outward current.

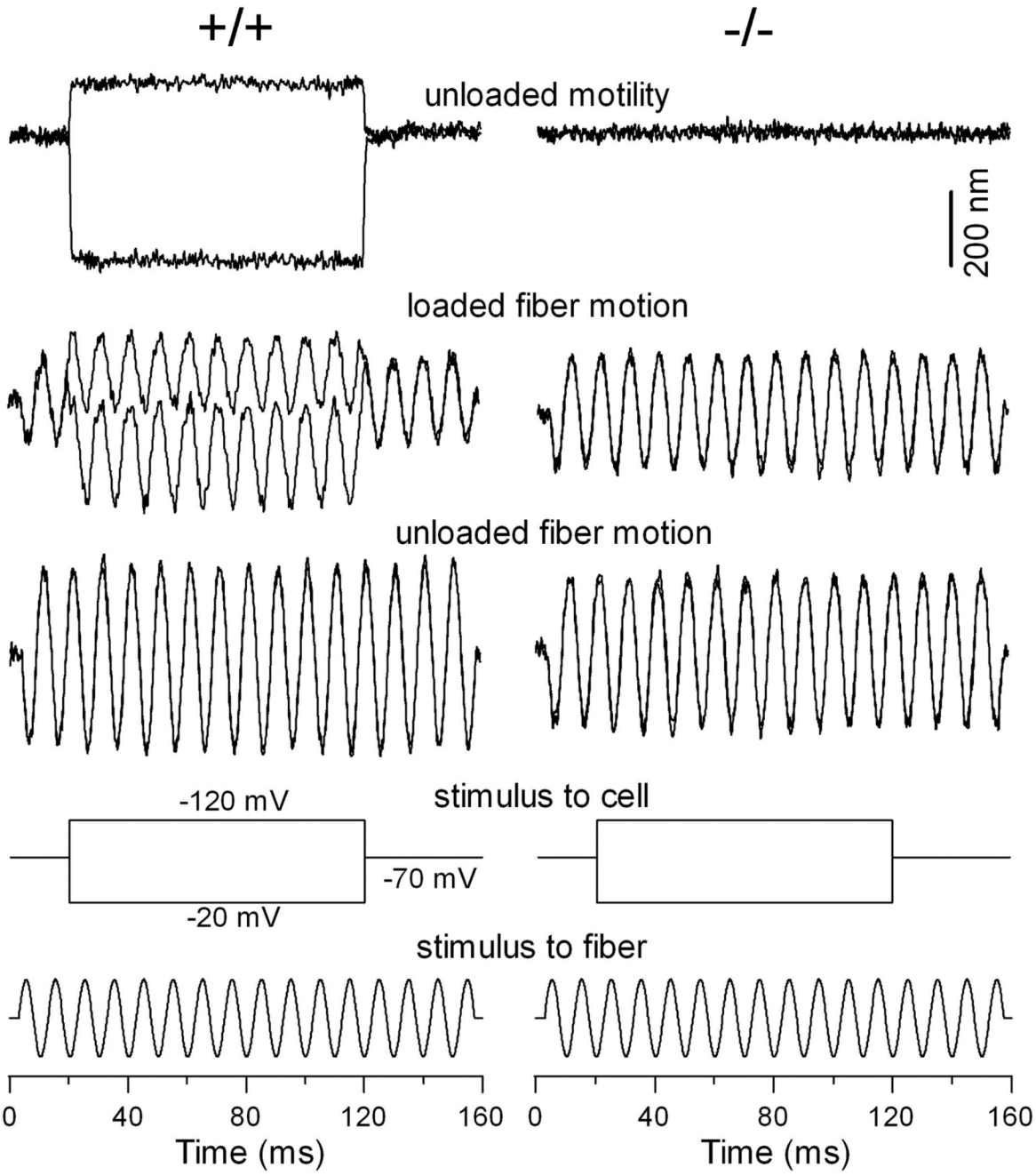


**Figure 7.**

Examples of somatic motility and voltage-dependent stiffness changes obtained from WT and prestin-null OHCs. Downward deflections represent depolarization (cell contraction). On the left panels, somatic motility and voltage-dependent stiffness change was observed. The motility showed larger contraction than elongation at the holding potential of −70 mV. The stiffness change is reflected by changes of the amplitude of the loaded-fiber motion during contraction or elongation of the cell. On the right panels, no motility was observed. Note that the amplitude of the loaded-fiber motion was not altered when motility was absent.